Phase Transformation Behavior of Al_2O_3 Scale Formed on Pt-modified γ'-Ni_3Al-based Alloys with and without Hf Addition

Shigenari Hayashi
Division of Materials Science and Engineering, Faculty of Engineering, Hokkaido University,
N13, W8, Kitaku, Sapporo, Hokkaido, 060-8628, Japan

Brian Gleeson
Department of Mechanical Engineering & Materials Science, University of Pittsburgh, Pittsburgh, PA, 15261, USA

Keywords: Hf effect, Al_2O_3 phase transformation, Grain growth, Short-term kinetics

Abstract

The allotropic phase transformation behavior of Al_2O_3 scale formed on Ni-22Al-30Pt (in at.%) with and without 0.5Hf was investigated during short-term (i.e., 3min dwell) cyclic oxidation at 1150ºC in air. Hafnium addition did not appear to affect the oxidation rate in the early oxidation cycles, but it did delay the phase transformation from the metastable θ-Al_2O_3 structure to the stable α-Al_2O_3. Small dimples, which corresponded to α-Al_2O_3 grains, started to form on the Hf-free alloy after only 3 oxidation cycles; whereas, no apparent morphological change of the oxide scale surface was observed on the Hf-modified alloy. The transformation to α-Al_2O_3 was found to initiate at scale/alloy interface on the Hf-free alloy, but it initiated at gas/scale interface on the Hf-modified alloy. Depth profiling using glow discharge optical emission spectroscopy revealed that Hf enriched at the scale/alloy interface due to Hf rejection associated with the formation of an Al-depleted γ-layer, which has a low Hf solubility. Higher positive strain energy due to Hf solution in the metastable Al_2O_3 was inferred to be the main contributor to the delayed the transformation.

Introduction

A number of high-temperature alloys and coatings rely on the formation of a continuous scale layer of aluminum oxide (Al_2O_3) for prolonged protection from surface degradation at elevated temperatures. This is because an Al_2O_3 scale has the requisite attributes of being both thermodynamically stable and slow growing. Several structural variants of Al_2O_3 have been reported to form during high temperature oxidation, and they are classified into the metastable κ- [1], γ- [2], and θ-Al_2O_3 [3] structures and the stable α-Al_2O_3. When alumina-scale forming alloys are exposed at elevated temperature to oxygen-containing environments, one or more metastable Al_2O_3 usually initially form, followed by the eventual transformation to α-Al_2O_3. The growth rate of a metastable Al_2O_3 scale is significantly faster than that of α-Al_2O_3 [4] and therefore rapid transformation to α-Al_2O_3 is deemed desirable to improving the overall oxidation resistance of the alloy or coating.

Small additions of reactive elements (REs) such as Y, Zr, and Hf, are known to improve Al_2O_3 scale adhesion and reduce the rate of Al_2O_3-scale growth [5-9]. Indeed, much attention has been directed to clarifying these beneficial effects [5,8,10]. However, only a limited amount of attention has been given to elucidating the effects of REs on the phase transformation to α-Al_2O_3 [11-16]. From those limited investigations, yttrium has been reported by some to slow the transformation to α-Al_2O_3 on Ni-based alumina-forming alloys during high-temperature oxidation [11,12,16]; whereas, other investigations have concluded that yttrium accelerates the transformation [14,15]. Jedliński [13] surmised that a relatively high content of yttrium addition to alumina-forming alloys retards the transformation, but a small content accelerates the transformation. There are only a few investigations on the effect of other reactive elements such as Hf and Zr on the transformation to α-Al_2O_3. Those investigations are also varied in their conclusions, i.e., these elements may accelerate [15], slow [11,17] or have no apparent effect [2] on the transformation to α-Al_2O_3.

The metastable → stable transformation behavior of Al_2O_3 has not been limited to the field of thermal oxidation. In fact, the allotropic phase transformation kinetics of Al_2O_3 has been frequently reported in catalysis studies. Here, it is desirable to maintain the metastable Al_2O_3 structures and hence prolong transformation to the stable α structure. On the basis of catalyst-related studies on thermally exposed oxide powders, it has been inferred that Mg accelerates and Zr, Hf, and Y slow the metastable → stable Al_2O_3 transformation [18-20].

Returning to the transformation of a thermally grown Al_2O_3 scale, it has been generally reported that nucleation of α-Al_2O_3 occurs at the scale/alloy interface during

oxidation of RE-free β-NiAl [21], γ'-Ni_3Al [22], NiAlPt, [23], NiCrAl [2, 4], and FeCrAl [24-26] systems. However, the trends reported are not without variance. For instance, Doychak and Rühle [27] reported that α nucleation occurs at the gas/scale interface for β-NiAl, which is contrary to the results reported by Yang *et al.* [21]. These latter authors inferred that the transformation to α-Al_2O_3 was due to heterogeneous nucleation and that defects at the scale/alloy interface provide preferential nucleation sites.

A complicating factor in the study of α-Al_2O_3 transformation in a thermally grown scale is the role played by minor and/or major alloying elements. The stable α-Al_2O_3 has a corundum crystal structure. Thus, other corundum-structured oxides, such as Cr_2O_3 and Fe_2O_3, can serve to facilitate α-Al_2O_3 nucleation, as has been reported for Fe- and Cr-containing alloys [4, 25, 26]. In those studies, cross-sectional TEM analysis strongly indicated that the α-Al_2O_3 nucleated initially at the scale/alloy interface.

The purpose of this study was to investigate the transformation behavior of Al_2O_3 scales formed on γ'-based Ni-Al-Pt alloys during very short oxidation exposures. The only alloy-constituent variable was Hf, thus allowing for a clearer interpretation of its effects on the eventual transformation to α-Al_2O_3.

Experimental Procedures

Pt-modified γ'-Ni_3Al-based alloys of nominal composition (in at.%) Ni-22Al-30Pt with and without 0.5 at.%Hf were prepared by argon-arc melting the pure (~99.99%) constituent metals. The alloys were drop-cast into the form of rods approximately 50 mm long and 13 mm in diameter and then subsequently homogenized in a vacuum environment at 1200ºC for 24h, followed by 1150ºC for 48h. Approximately 1.5 mm thick test samples were cut from the homogenized rods and then ground to a 1200-grit finish using SiC abrasion paper. The samples were then polished a 3μm finish using diamond paste. Fiduciary marks, 20-40 microns in size, were impressed on the surfaces of the samples using a micro-hardness indenter (50 g load). Use of these marks enabled characterization of the scale-surface evolution at the same location. All samples were ultrasonically cleaned in acetone at the completion of preparation and then kept in a desiccator for up to 24h until used for oxidation testing.

In the present study, a very short-term cyclic oxidation was chosen in order to observe the development of oxide scale and the progress of the metastable → stable Al_2O_3 phase transformation. Cyclic oxidation experiments were performed using an open, vertical furnace equipped with a timer-controlled sample elevation unit that has been described elsewhere [17]. Samples were hooked to an Al_2O_3 rod and then

automatically raised into the furnace hot zone, which was kept at 1150ºC. The time to reach the reaction temperature of 1150ºC was about 300 s and, at the end of a given dwell at 1150ºC, the samples were automatically lowered to a position below the furnace tube and allowed to air-cool to room temperature. In the present study, the 1150°C dwell for the first cycle was 1 min, followed by 3min for the following 38 cycles (for a total of 115min at 1150°C). The sample temperature was measured using an R-type thermocouple located adjacent to the sample surface.

Sample mass was measured before and after exposure to a given number of thermal cycles using an analytical balance. Surface morphologies were observed using a field emission scanning electron microscope (FE-SEM). A focused ion beam (FIB) system with a Ga ion source was used for the preparation of the TEM samples. Element distributions were measured as a function of depth from the sample surface using glow discharge optical emission spectroscopy (GD-OES). Phase identification of the initially-formed Al_2O_3 scale was carried out by electron diffraction and XRD and Raman spectroscopy.

Results

Oxidation kinetics

Figure 1(a) shows the early-stage 1150ºC cyclic-oxidation kinetics (3 mins/cycle) of Ni-22Al-30Pt with and without 0.5%Hf addition. The same data are re-presented in Fig. 1(b) and compared to corresponding isothermal oxidation kinetics at 1150ºC [17]. The isothermal and cyclic behaviors are seen to be comparable. Focusing solely on the cyclic-oxidation kinetics behavior, the oxidation rates for both samples were similar and very rapid for about the first four cycles and then decreased slightly with continued oxidation. The oxidation rate of the Hf-free alloy rapidly decreased after around six cycles, while the Hf-containing alloy continued to oxidize at a relatively fast rate. It wasn't until about 36-39 cycles that the oxidation rate of the Hf-containing alloy significantly decreased. A comparison of the data in Fig. 1(b) suggests that thermal cycling of the Hf-containing alloy delayed its transition to very slow oxidation kinetics. Further, and for both alloys, the transition to slower oxidation kinetics was apparently independent of the oxidation condition (*i.e.*, isothermal *vs.* cyclic), and was instead dependent on the oxidation mass gain, which in turn corresponds to a particular scale thickness. This critical mass gain was different for the two alloy compositions. Specifically, transition to slower kinetics occurred when the oxidation mass gain reached about 0.16 and 0.07 mg/cm^2 for Hf-containing and Hf-free alloys, respectively.

Surface morphologies

Figure 2 shows the surface morphologies of the Hf-free alloy after various oxidation cycles, while Fig. 3 shows enlarged images of the marked areas in Fig. 2. The narrow square boxes inserted in Figs. 3d, f and 5d, f indicate the positions taken for cross-sectional TEM samples prepared by FIB. The square shaped holes seen in Figs 2e and 4e are the areas milled by FIB. Except for the alloy oxidized for 39 cycles, fiduciary marks were used to obtain images from the same area of the alloy surface during the course of the oxidation exposure. A different sample was used for the 39 cycles exposure in order to arrive at a more thorough microstructural characterization. Close inspection of Fig. 2 reveals that small dimples formed on the oxidized surface after 3 cycles, with the number density of those dimples depending on the orientation of the underlying alloy grain. In the SEM images, the dimples evolved into higher-contrast globules that increased in size with increasing oxidation cycles (starting from 5 cycles). After 39 cycles, which correspond to a total of 115 min of oxidation exposure, almost the entire surface was covered by the high-contrast globules. From the higher magnification images in Fig. 3(f), a network-like structure was found to have developed after 39 oxidation cycles in the areas where the globules were present, while needle- or platelet-like oxides were observed in those regions of the surface that had a darker contrast.

As shown in Figs. 4 and 5, no high-contrast globules were observed in the scales formed on the Hf-modified alloy, even after 39 oxidation cycles. The scale surface was relatively smooth up to 11 cycles, but small dark regions widely distributed over the entire surface were found to be present after three cycles (see enlarged images in Fig. 5). The formation and distribution of these dark-spotted regions depended upon the alloy grains, and tended to be densely formed along the alloy grain boundaries. The total number of these spots appeared to remain constant with different oxidation cycles. Moreover, SEM observation using different accelerating voltages of 5 and 15 keV confirmed that these spots formed beneath the oxide scale. After 39 oxidation cycles, the scale surface became rough, but a couple of smooth areas, indicated by the arrows in Fig. 5(f), were found to form.

TEM cross-sections

Figures 6 and 7 show TEM cross-sections of the Hf-free alloy after 7 and 39 cycles of oxidation, respectively. These TEM samples were taken from the rectangular areas indicated in the surface images shown in Fig. 3(d) and (f). The oxide scale after 7 cycles consisted of two parts: coarse equiaxed grains (indicated by arrows in Fig. 6(a))

and fine columnar grains. The size of the equiaxed grains after 7 cycles was about 500nm; whereas, the columnar grains were less than several nanometers. The size and distribution of the equiaxed grains correspond to the bright granular features that were observed on the sample surfaces (see Fig. 3). The fine columnar grains grew throughout the oxide scale, while the coarse equiaxed grains formed in regions along the scale/alloy interface. Electron diffraction analysis revealed that these equiaxed grains were α-Al_2O_3. The size of the columnar grains was too small to allow for accurate structural determination using electron diffraction. However, complementary analyses using Raman spectroscopy revealed that the columnar grains were θ-Al_2O_3. Thus, the fine columnar grains in Figs. 6 and 7 are inferred to be metastable θ-Al_2O_3. The dark-field image in Fig. 6(c), confirms the distinct, relatively coarse-grain nature of the α-Al_2O_3. In areas that the α-Al_2O_3 grains formed, the oxide scale tended to be thinner, which may be attributable to the volume reduction associated with the $\theta \rightarrow \alpha$-$Al_2O_3$ transformation [26] and the subsequent slower growth rate of the α-Al_2O_3 scale. The coarse α-Al_2O_3 grains tended to grow laterally and eventually merge with one another to the extent that they covered the entire alloy surface after 39 cycles, as indicated in Fig. 7. Except for some areas where θ-Al_2O_3 remained above the α-Al_2O_3 layer (see Fig. 7b), the oxide scale completely transformed to α-Al_2O_3 by 39 cycles. In the fully transformed regions, the oxide scale consisted of only large single grains. The fully transformed α-Al_2O_3 scale was thicker at the oxide grain boundaries than at intragrain areas. Further, the α-Al_2O_3 grain boundaries corresponded to the ridges of the network-like structure observed on the oxide surface see (Fig. 3(f)).

TEM cross-sections of the Hf-containing alloy after 7 and 39 cycles are shown in Figs. 8 and 9, respectively. The TEM specimens were taken from the indicated areas of the surface images of Fig. 5(d) and (f). The oxide scale consisted of fine columnar θ-Al_2O_3 grains, as confirmed by Raman spectroscopy, and no α-Al_2O_3 grains were found after 7 oxidation cycles. Relatively large voids were found at the oxide/alloy interface. These voids correspond to the dark spots observed in the surface images (see Fig. 5). The oxide scale thickness above the voids was thinner than other areas. Moreover, thin oxide scale was found to form on the void surface, indicating that the partial pressure of oxygen in a void eventually increased to a level sufficient to form new oxide beneath the Al_2O_3 scale. Void surfaces, *i.e.*, the scale/alloy interface of voids, were very smooth and faceted. After 39 oxidation cycles, the oxide scale grew thicker, but still consisted of mostly fine θ-Al_2O_3 columnar grains. The scale/alloy interface became very non-planar due to the formation of and subsequent oxidation within the interfacial voids. The oxide scale that formed in the voids also

grew thicker, but the voids were not completely filled by newly formed oxide. There were small equiaxed grains that formed locally on the external surface of the oxide scale, and these were identified by electron diffraction to be α-Al_2O_3. These α-Al_2O_3 grains were much smaller, ~150nm, than those formed on the Hf-free alloy, ~1.2μm. Below the small α-Al_2O_3 grains, θ-Al_2O_3 columnar grains still remained after 39 oxidation cycles.

Discussion

Void formation

Large voids were observed on only the Hf-containing alloy. Although many previous studies of Al_2O_3-forming alloys indicated that the void formation was suppressed by REs additions [28], Hf addition in the present study did not suppress the void formation. The distribution and number of voids were clearly seen to have an orientation relation with the γ'-substrate, as seen by black dots in Fig. 5b and c. Moreover, these voids tend to form along grain boundaries of substrate. This result may indicate that the void formation is linked to the selective removal of Al from the alloy to form Al_2O_3, i.e., the Kirkendall effect. Since metastable Al_2O_3 is known to grow primarily by the outward migration of Al^{3+}, and the transformation to α-Al_2O_3 was significantly delayed on the Hf-containing alloy, a relatively large number of voids was able to form in Hf-containing alloy. The faceted nature of the voids formed supports this speculation that the voids formed during the oxidation process rather than during cooling. Further discussion on void formation is beyond the scope of the present paper.

α-Al_2O_3 formation

The θ-Al_2O_3 → α-Al_2O_3 transformation in the scales formed on the Hf-free and Hf-containing $\gamma+\gamma$' alloys occurred in different manners and at different rates. In particular, the transformation was considerably delayed for the Hf-containing alloy. In the case of the Hf-free alloy, α-Al_2O_3 grains, which were observed as white spots in Fig. 2, formed by at least 3 oxidation cycles. In this case, the number of α-Al_2O_3 grains increased with time and grew particularly quickly in the lateral directions. The white spots corresponding to α-Al_2O_3 grains were not observed on the Hf-containing alloy until 39 oxidation cycles. Even then the α-Al_2O_3 grains were quite small and eqiaxed, and the oxide scale was still predominately comprised of fine columnar θ-Al_2O_3 grains.

As mentioned in the Introduction, many previous studies inferred that the metastable → α-Al_2O_3 transformation is initiated at the scale/alloy interface. In

agreement with those previous studies, it was found in the present study that the nucleation of α-Al_2O_3 occurred at scale/alloy interface of the Hf-free $\gamma+\gamma'$ alloy. By contrast, nucleation of α-Al_2O_3 was found to initiate at the gas/scale interface of the Hf-containing alloy. In terms of the effects of REs on the metastable $\rightarrow$ α-Al_2O_3 transformation, Burtin *et al.* [18] found from a study on Al_2O_3 powders that elements which have a larger ionic radius and/or higher cation valency compared to Al^{3+}, tend to delay the transformation to α-Al_2O_3. For instance, they found that Zr significantly delayed the transformation. There are no data available for the effects of Hf on transformation of Al_2O_3, however, Hf has a large ionic radius, 0.85 Å, very similar to Zr, 0.86Å [30]. Therefore, it is reasonable to conclude that Hf has a similar effect as Zr in delaying the transformation to α-Al_2O_3. Specifically, the ~8% volume reduction that is associated with the $\theta \rightarrow \alpha$ transformation (α has a smaller unit cell) would be impeded by the presence of a relatively large cation like Hf^{4+} or Zr^{4+}. In the context of energetics, the reason for Hf (or Zr) delaying the α-Al_2O_3 formation is inferred to be a decrease in driving force for the transformation due to a disproportionate increase in the Gibbs free energy of α-Al_2O_3 by larger size cation doping. This disproportionate increase is due the expected higher solubility of Hf in θ compared to α, i.e., the positive strain energy of having Hf (or Zr) in solution would increase the Gibbs free energy of α more than θ.

Figure 10 shows a cross-sectional microstructure and the corresponding GD-OES concentration profiles of each element of the Hf-containing alloy after 30min of isothermal oxidation. Hf was detected through the entire oxide scale by GD-OES analysis. Moreover, an aluminum depleted γ-Ni(Al, Pt, Hf) layer was formed just below the oxide scale due to the selective removal of Al from the substrate to form the Al_2O_3 scale. Hafnium solubility in γ is much lower than that in γ' [31-33]. For instance, Mu *et al.* [33] found that the partitioning coefficient of Hf, $k_{\mathrm{Hf}} = C_{\mathrm{Hf}\gamma}/C_{\mathrm{Hf}\gamma'}$, is less than 0.1 in high Pt content $\gamma+\gamma'$ alloys. Accordingly, Hf must be rejected when the Al-depleted γ layer is formed in the subsurface region. The rejected Hf diffuses to both into the γ'-substrate and to the scale/alloy interface. Consequently, the Hf becomes enriched at the interfaces of the subsurface γ layer, so that the scale in contact with this γ layer becomes enriched to some extent with Hf. Such an outcome is indicated in the Hf profile in Fig. 10b. In this figure, the Al_2O_3/alloy interface is defined as the position where Al and Ni contents were both at 50at%. It is seen that the Hf content decreased in the subsurface γ layer and there is Hf enrichment at the Al_2O_3/alloy interface (Fig. 10b). From the cross-sectional micrograph in Fig. 10a it is seen that this enriched Hf did not oxidize to HfO_2. Rather, the Hf is probably in Al_2O_3 solid solution, even though HfO_2 is thermodynamically more stable than Al_2O_3.

According to Mu *et al.* [33], Pt decreases the chemical activity of Hf to the extent that the Hf:Pt atom ratio in γ must to be greater than ~0.02 for HfO_2 formation to be stable. This ratio was apparently not reached in the sample shown in Fig. 10. Even so, there was clear Hf enrichment at the Al_2O_3/alloy interface and it is postulated that this enrichment delayed the α-Al_2O_3 nucleation at the scale/alloy interface relative to the Al_2O_3/gas interface, where the Hf content was much less, Fig. 10b. Thus, while a driving force for the θ→α transformation undoubtedly existed at the scale/alloy and scale/gas interfaces, the higher strain energy brought about by the greater Hf enrichment at the former interface led to α-Al_2O_3 nucleation being favored at the scale/gas interface. Interestingly, once the θ→α transformation occurs at a given interface, the other interface does not show the transformation to any measureable extent. The reason for this observation is that the compressive strains in the θ associated with the volume reduction concomitant with the θ→α transformation [34] contribute to promote further transformation. Stated differently, once α forms, its continued transformation at the transformation front is favored. Any further discussion on this aspect of the current results would require data that are currently not available.

Subsequent growth of α-Al_2O_3 grains

Figure 11 presents re-arranged images from Figs. 7b and 9b in order to compare cross-sectional microstructures formed on Hf-free and Hf-containing alloys after total 115min of oxidation. The grain size of α-Al_2O_3 formed on the Hf-containing alloy was much smaller than that formed on the Hf-free alloy; although, in both cases, the α-Al_2O_3 grains were much larger than the columnar θ-Al_2O_3 grains. Further, in a previous study [17], we reported that the growth rates of α-Al_2O_3 scale (after complete transformation occurred) on both alloys were very slow. In particular, the growth rate in the intragranular regions of α-Al_2O_3 on the Hf-free alloy (*i.e.*, growth via lattice diffusion) was extremely slow. Indeed, the growth rate of the α-Al_2O_3 grains during the θ→α transformation was apparently much faster than the scale growth rate. Rapid grain growth was reported during heat treatment of metastable Al_2O_3 powder in a catalysis study and was proposed to be attributed to low α-Al_2O_3 nucleation density coupled with the fast consumption of θ-Al_2O_3 associated with the α-Al_2O_3 formation [35]. This mechanism can be applied to the current observations. Based on the surface and cross-sectional images obtained, the number of α-Al_2O_3 nuclei was higher for the Hf-containing alloy, which is in accordance with the delayed α nucleation observed with this alloy, *i.e.*, nucleation rate tends to be inversely proportional to incubation time for nucleation [29]. Since grain growth essentially

stopped at the point of grain impingement, the α-Al_2O_3 grain size in the scale formed on the Hf-containing alloy was much smaller than in the scale formed on the Hf-free alloy.

The oxidation mass gain at which the $\theta \rightarrow \alpha$ transformation occurred was larger for the Hf-containing alloy (0.16 mg/cm^2) than for the Hf-free alloy (0.07 mg/cm^2). This may be simply attributed to the delayed $\theta \rightarrow \alpha$ transformation in the case of the former alloy, but the mass gains at which the transformations occurred were similar for the alloys when oxidized under isothermal conditions (see Fig. 1(b)). It is possible that the thermal stresses imposed in the scales during cyclic oxidation influenced the $\theta \rightarrow \alpha$ transformation to different extents; however, a more systematic study would be needed to expand upon this speculation.

Summary

The transformation behavior of Al_2O_3 scale formed on $\gamma+\gamma'$ Ni-22Al-30Pt with and without 0.5Hf during very short-time cyclic oxidation was investigated. The results obtained may be summarized as follows.

1. The θ-$Al_2O_3 \rightarrow \alpha$-$Al_2O_3$ transformation occurred by about 3 cycles on the Hf-free alloy, but occurred by about 39 cycles on the Hf-containing alloy. Thus, Hf significantly delays the $\theta \rightarrow \alpha$ transformation.
2. In agreement with the majority of previous studies reporting the $\theta \rightarrow \alpha$ transformation, α-Al_2O_3 nucleation began heterogeneously at the scale/alloy interface in the case of the Hf-free alloy. However, the present results clearly show that the preferred $\theta \rightarrow \alpha$ transformation site becomes the gas/scale interface for the Hf-containing alloy. Rapid grain growth, which was much faster than the scale growth rates, was observed after nucleation of α-Al_2O_3 grains.
3. Hf enrichment was observed at the scale/alloy interface, and the positive strain energy associated with this enrichment is considered to be the reason for the change in location of the initial nucleation of α-Al_2O_3 to the scale/gas interface.
4. The final α-Al_2O_3 grain size was considerably smaller in the scale formed on the Hf-containing alloy than that formed on the Hf-free alloy. This is due to a greater α-Al_2O_3 nuclei density eventuating in the Hf-containing scale as a consequence of the greater incubation period for nucleation.

Acknowledgments

Partial support for this work was provided by the Office of Naval Research, contract number N000140911127, with Dr. David Shifler being the Program Manager.

References

[1] D.B. Lee, H. Habazaki, A. Kawashima, and K. Hashimoto, Corr. Sci., 42, (2000), 721-729.

[2] J.L. Smialek and R. Gibala, Metall. Trans. A, 14A, (1983), 2143-2161.

[3] G.G. Rybicki and J.L. Smialek, Oxidation of Metals, 31, (1989) 275-304.

[4] M.W. Brumm and H.J. Grabke, Corr. Sci., 33, (1992), 1677-1690.

[5] J. Stringer, Mater. Sci. and Eng., A120, (1989), 129-137.

[6] R. Prescott and M.J. Graham, Oxid. Met., 38, (1992), 233-254.

[7] S. Mrowec, J. Jedlinski, and A. Gil, Mater. Sci. Eng. A120, (1989), 169-173.

[8] D.P. Moon, Mater. Sci. and Tech., 5, (1989), 754-764.

[9] D.P. Whittle and J. Stringer, Phil. Trans. R. Soc. Lond. A 295, (1980), 309-329.

[10] J. Jedlinski, Corr. Sci., 35, 5-8, (1993), 863-869.

[11] B.A. Pint, J.R. Martin, and L.W. Hobbs, Solid State Ionics, 78, (1995), 99-107.

[12] P.A. van Manen, E.W.A. Young, D. Schalkoard, C.J. Van der Wekken, and J.H.W de Wit, Surf. Interface Analy., 12, (1988), 391-396.

[13] J. Jedliński, Oxid. Met., 39, (1993), 55-60.

[14] R. Cueff, H. Buscail, E. Caudron, C. Issartel, and F. Riffard, Corros. Sci., 45, (2003), 1815-1831.

[15] I. Rommerskirchen and V. Kolarik, Mater. and Corr., 47, (1996), 625-630.

[16] D. Toma, W. Brandl, and U. Köster, Surf. Coat. Tech., 120-121, (1999), 8-15.

[17] S. Hayashi and B. Gleeson, Oxid. Met., 71, (2009), 5-19.

[18] P. Burtin, J.P. Brunelle, M.Pijolat, and M. Soustelle, App. Catalysis, 34, (1987), 225-238.

[19] P. Burtin, J.P. Brunelle, M.Pijolat, and M. Soustelle, App. Catalysis, 34, (1987), 239-254.

[20] M. Pijolat, M. Dauzat and M. Soustelle, Thermochimica Acta, 122, (1987), 71-77.

[21] J.C. Yang, E. Schumann, I. Levin, and M. Rühle, Acta Mater., 46, (1998), 2195-2201.

[22] E. Schumann, G. Schnotz, K.P. Trumble, and M. Rühle, Acta Metall. Mater., 40, (1992), 1311-1319.

[23] H. Svensson, J. Angenete, and K. Stiller, Surf. And Coat. Tech., 177-178, (2004), 152-157.

[24] S. Taniguchi and A. Andoh, Oxid. Met., 58, (2002), 545-562.

[25] P.Y. Hou, Anuu. Rev. Mater. Res., 38, (2008), 275-298.

[26] X.F. Zhang, K. Thaidigsmann, J. Ager and P.Y. Hou, J. Mater. Res., 21, (2006),

1409-1419.
[27] J. Doychak and M. Rühle, Oxid. Met., 31, (1989), 431-452.
[28] B.A. Pint, Oxid. Met., 45, (1997), 1-37.
[29] D.A. Porter and K.E. Easterling, Phase Transformation in Metals and Alloys, 2nd Ed. CRC press, UK, (1992).
[30] R.D. Shannon, Acta Cryst., A32, (1976), 751-767.
[31] R.R. Nagarajan, A.K. Jena, and R.K. Ray, Z. Metallkd., 88, (1997), 87-90.
[32] C. Zhang, J. Zhu, Y. Yang, H.-B. Cao, F. Zhang, W.-S. Cao, and Y.A. Chang, Intermetellics, 16, (2008), 139-147.
[33] N. Mu, T. Izumi, L. Zhang, and B. Gleeson, Proceedings to *Superalloys 2008*, The Minerals, Metals and Materials Society, (2008), 629-637.
[34] P.Y. Hou, A.P. Paulikas, and B.W. Veal, Mater. Sci. Forum, 522-523, (2006), 433-440.
[35] R.B. Bagwell, G.L. Messing, and P.R. Howell, J., Mater. Sci., 36, (2001), 1833-1841.

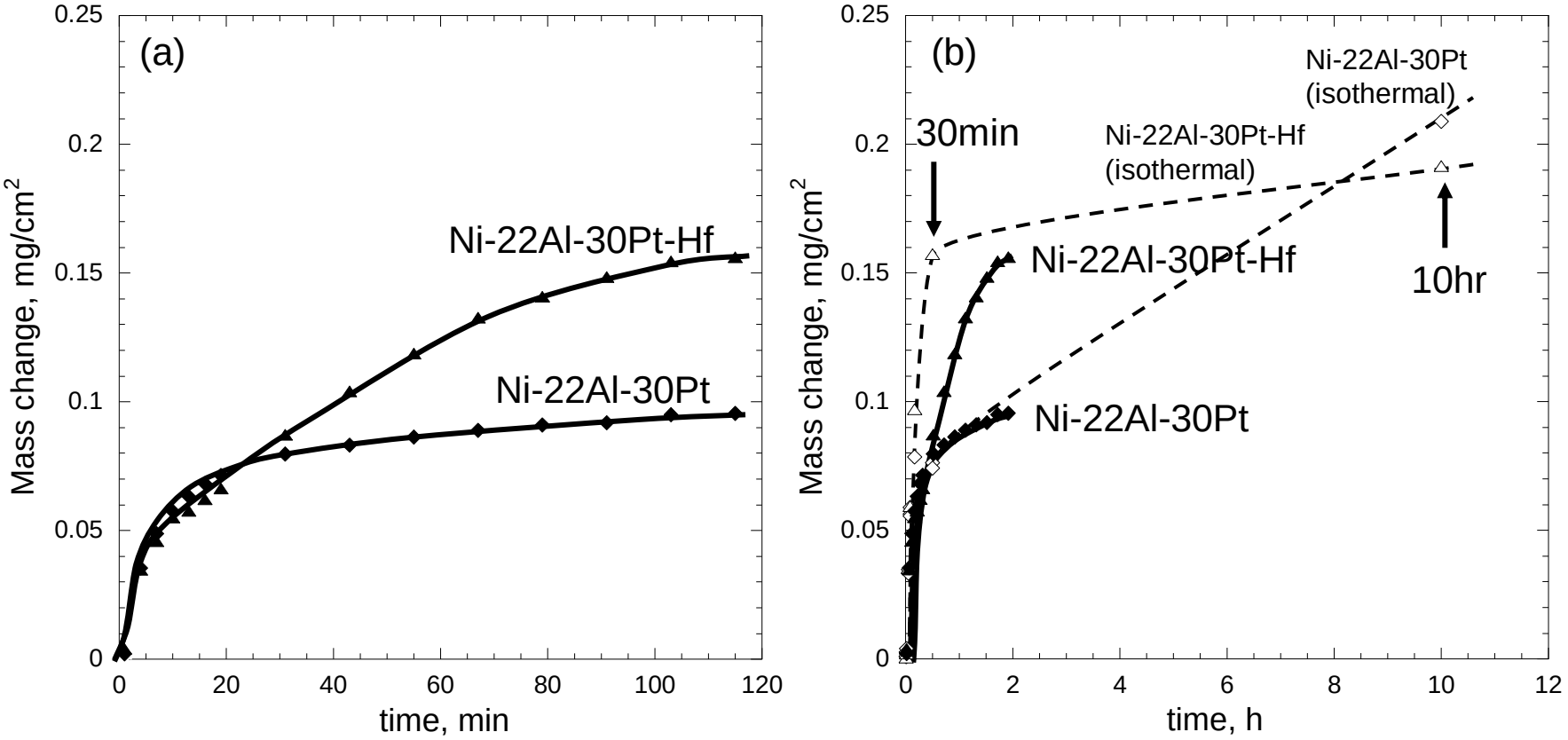

Fig. 1 Cyclic Oxidation kinetics of Ni-22Al-30Pt alloys with and without Hf
(a) cyclic oxidation behavior up to 39 cycles (115min), (b) comparison with isothermal oxidation results

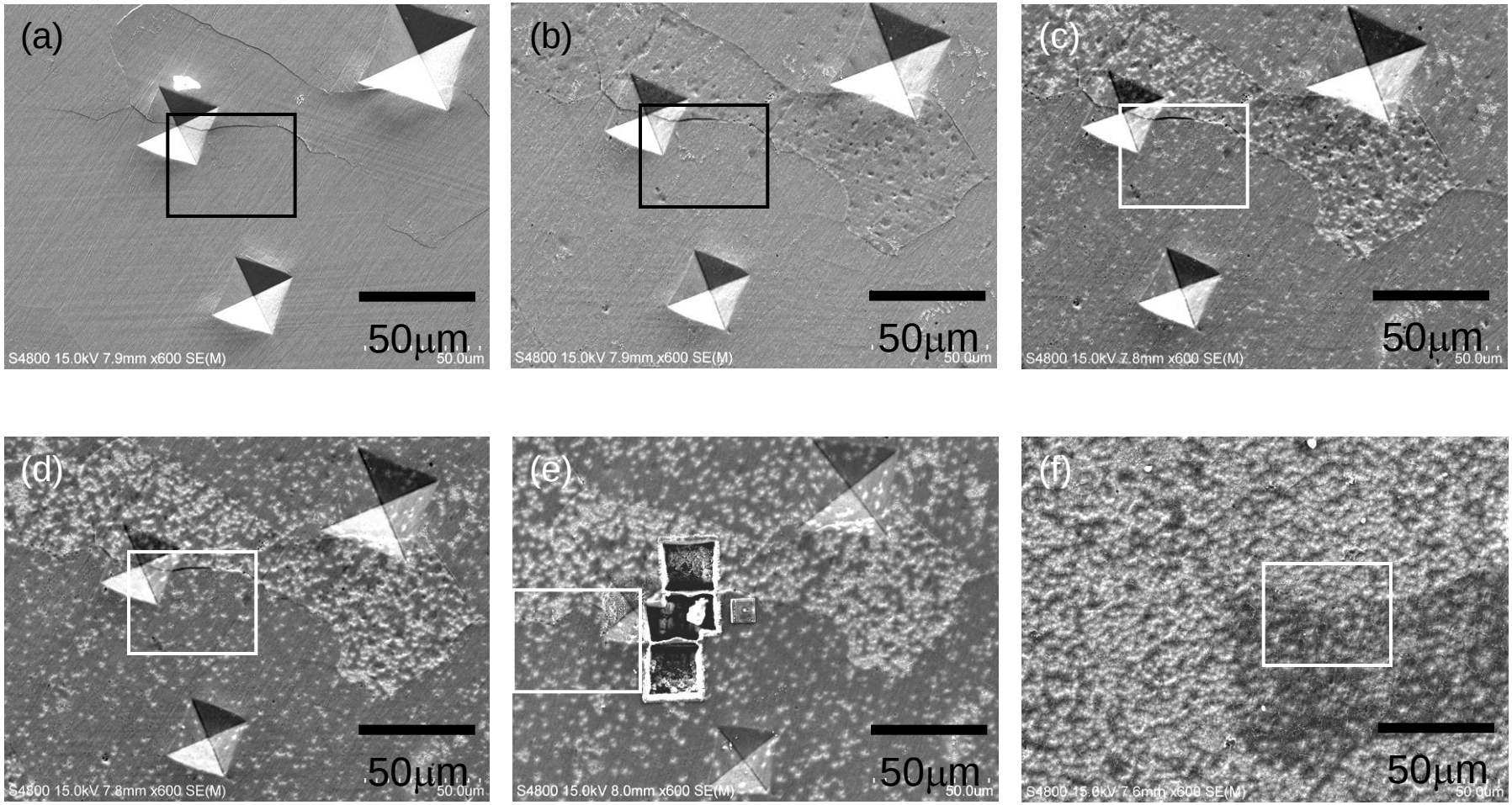

Fig. 2 Change in surface morphology of the Hf-free alloy after (a) 1 (1min), (b) 3 (7min), (c) 5 (13min), (d) 7 (19min), (e) 11 (31min), and (f) 39 (115min) cycles of oxidation.

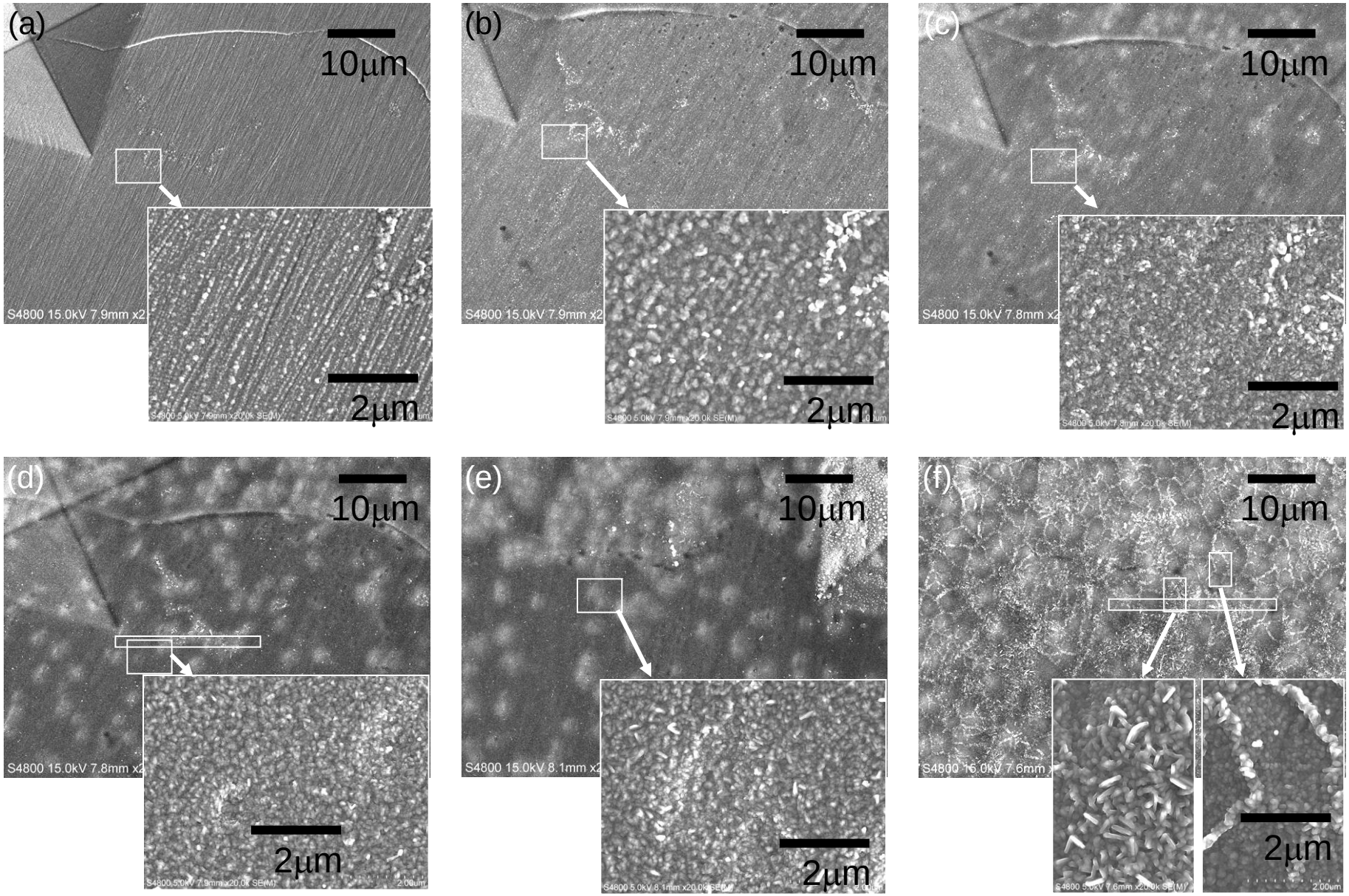

Fig. 3 Enlarged surface morphologies of the Hf-free alloy after (a) 1 (1min), (b) 3 (7min), (c) 5 (13min), (d) 7 (19min), (e) 11 (31min), and (f) 39 (115min) cycles of oxidation.

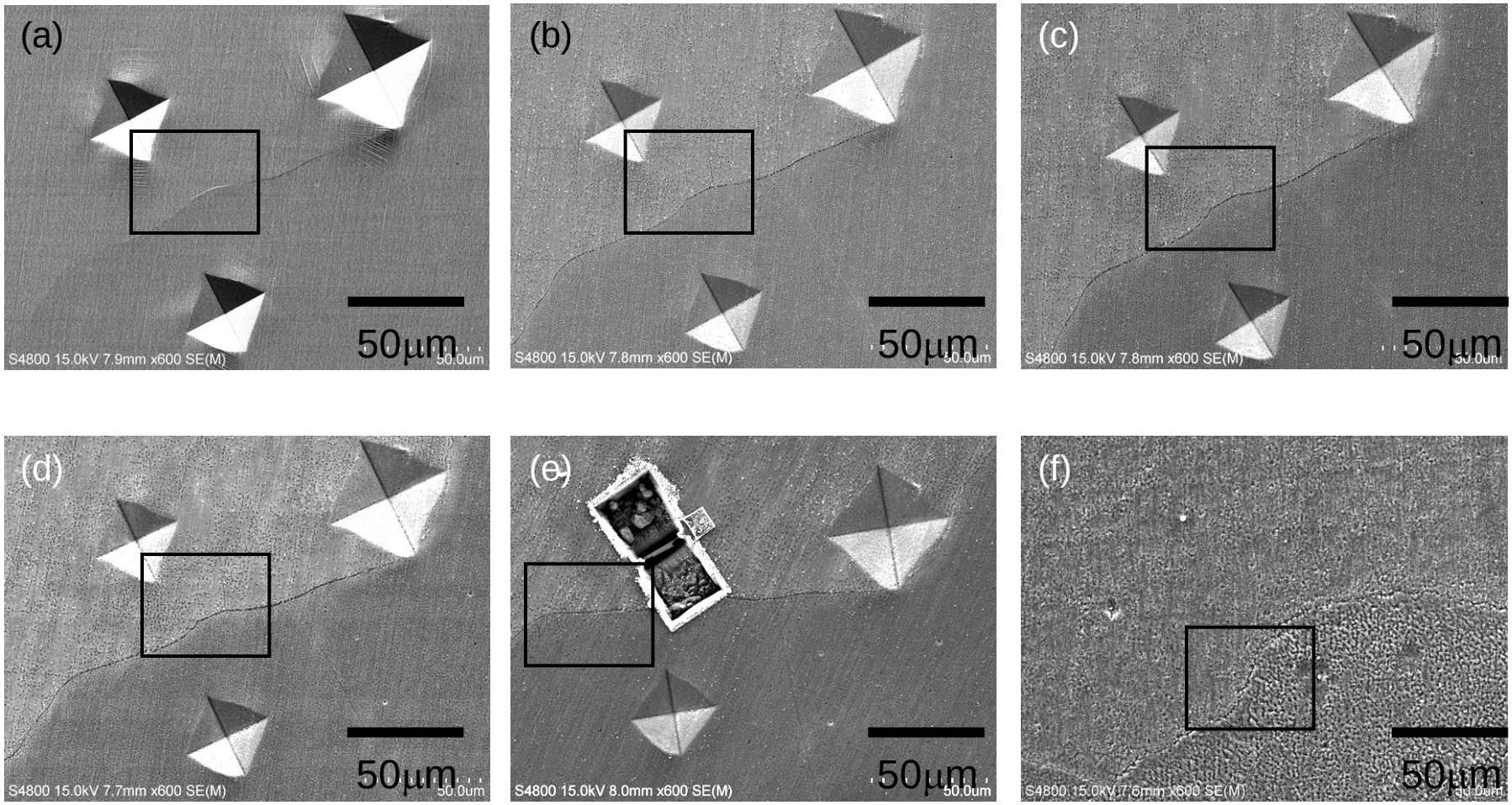

Fig. 4 Change in surface morphology of the Hf-modified alloy after (a) 1 (1min), (b) 3 (7min), (c) 5 (13min), (d) 7 (19min), (e) 11 (31min), and (f) 39 (115min) cycles of oxidation.

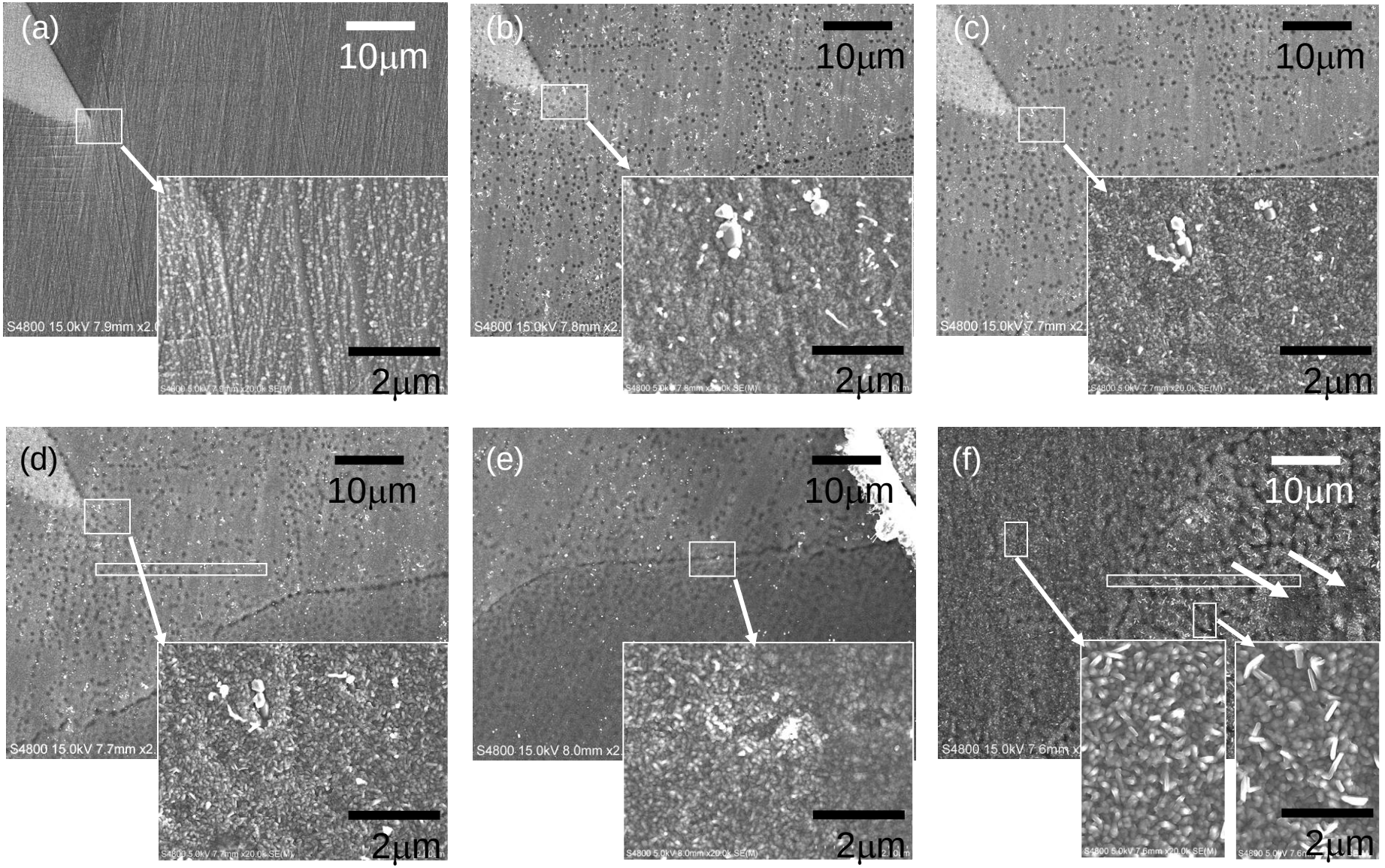

Fig. 5 Enlarged surface morphologies of the Hf-modified alloy after (a) 1 (1min), (b) 3 (7min), (c) 5 (13min), (d) 7 (19min), (e) 11 (31min), and (f) 39 (115min) cycles of oxidation.

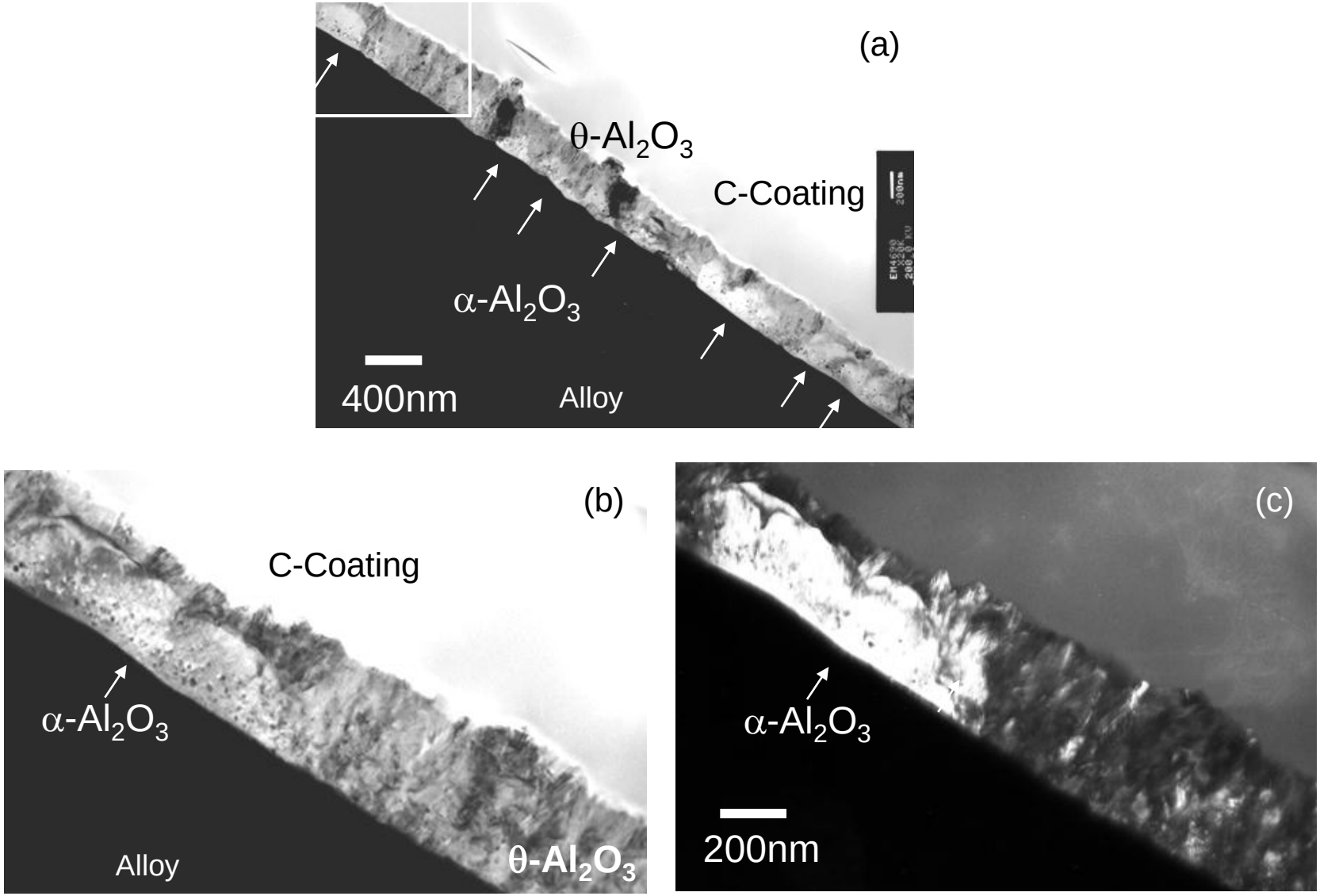

Fig. 6 TEM cross-sections of the Hf-free alloy after 7 oxidation cycles (19min total) at 1150°C in air. (b) is a enlarged view of the rectangular area in (a), and (c) is the dark field image of (b).

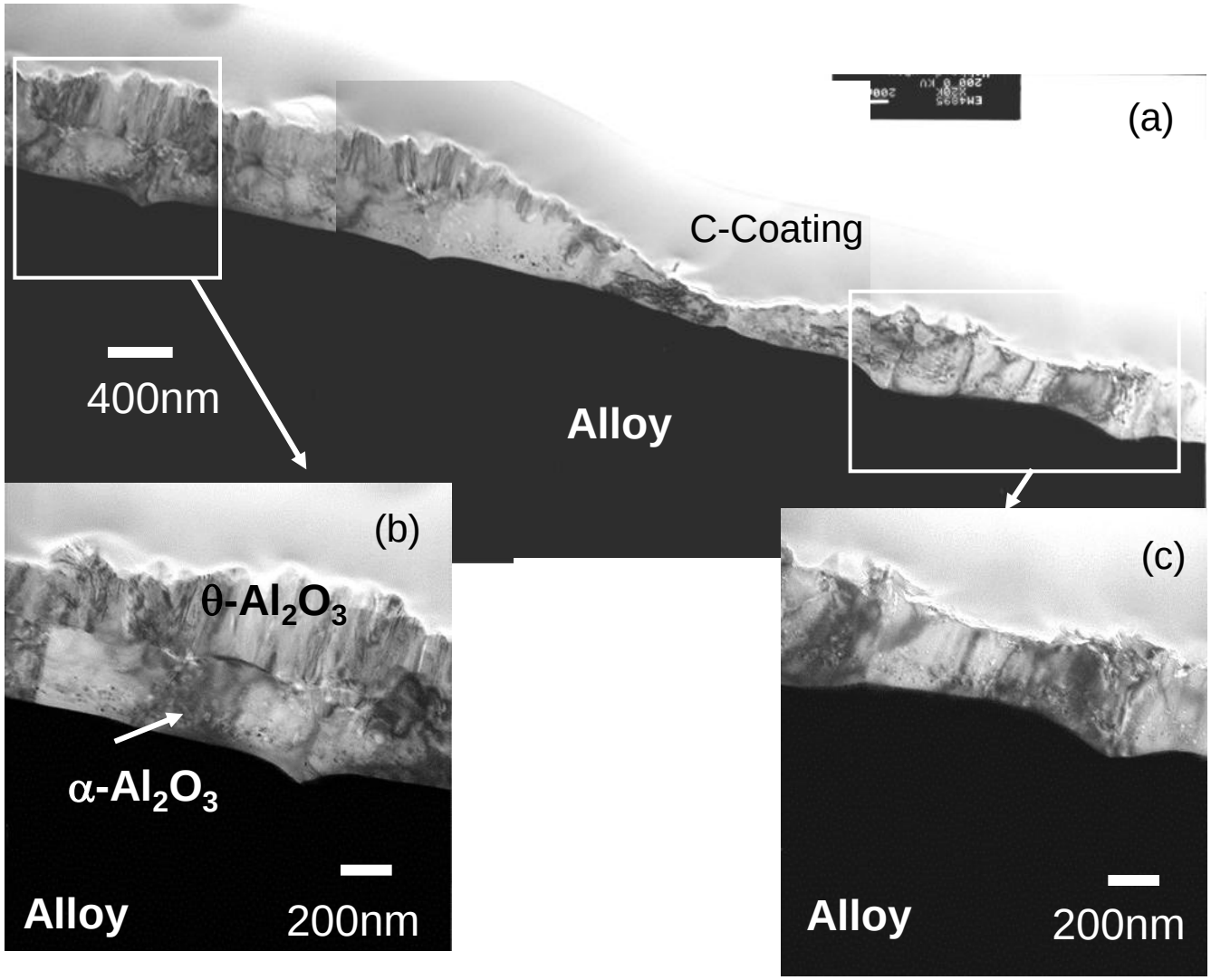

Fig. 7 TEM cross-sections of Hf-free alloy after 39 oxidation cycles (115min total) at 1150°C in air. (b), (c) are enlarged views of the rectangular areas in (a).

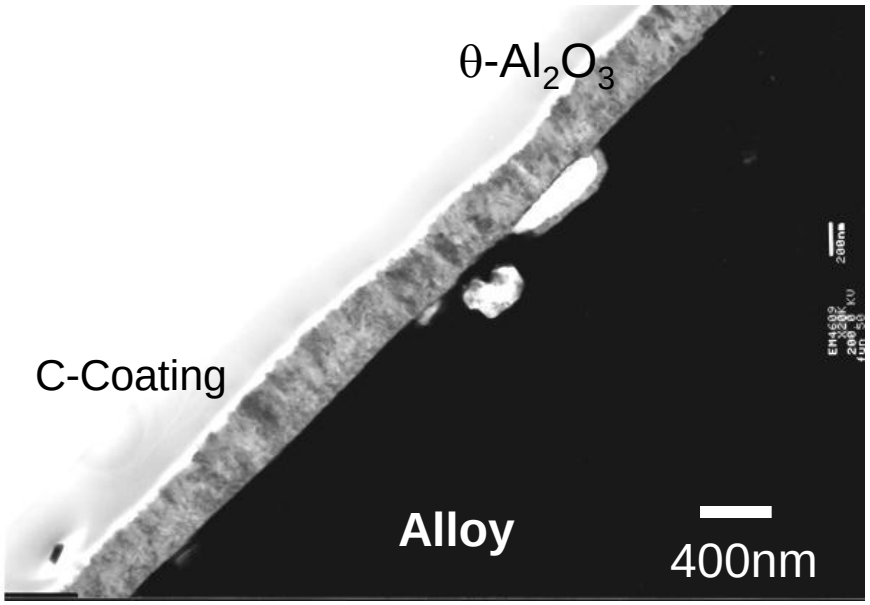

Fig. 8 TEM cross-sections of the Hf-modified alloy after 7 oxidation cycles (19min total) at 1150°C in air

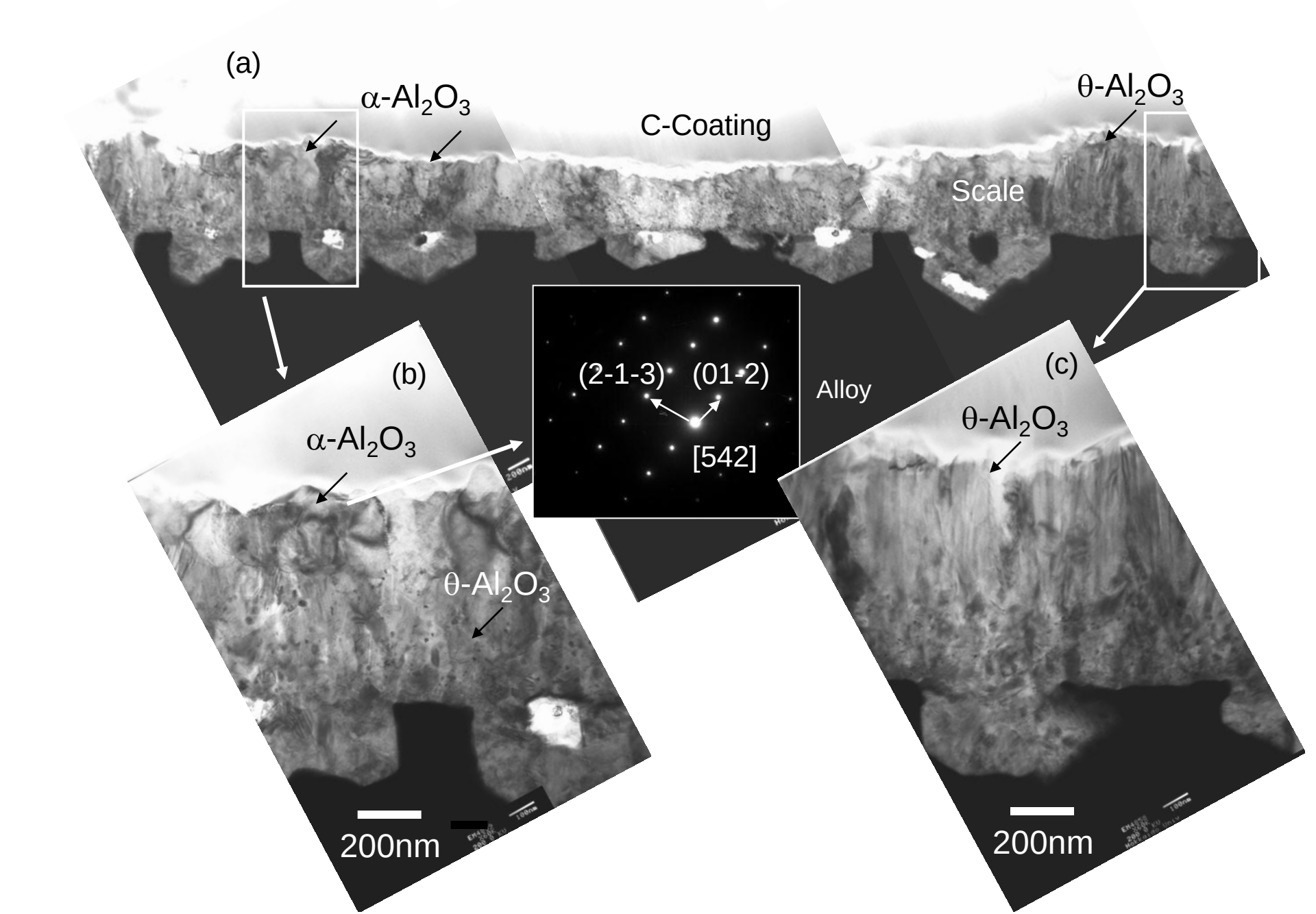

Fig. 9 TEM cross-sections of the Hf-modified alloy after 39 oxidation cycles (115min total) at 1150°C in air. (b), (c) are enlarged views of the rectangular areas in (a).

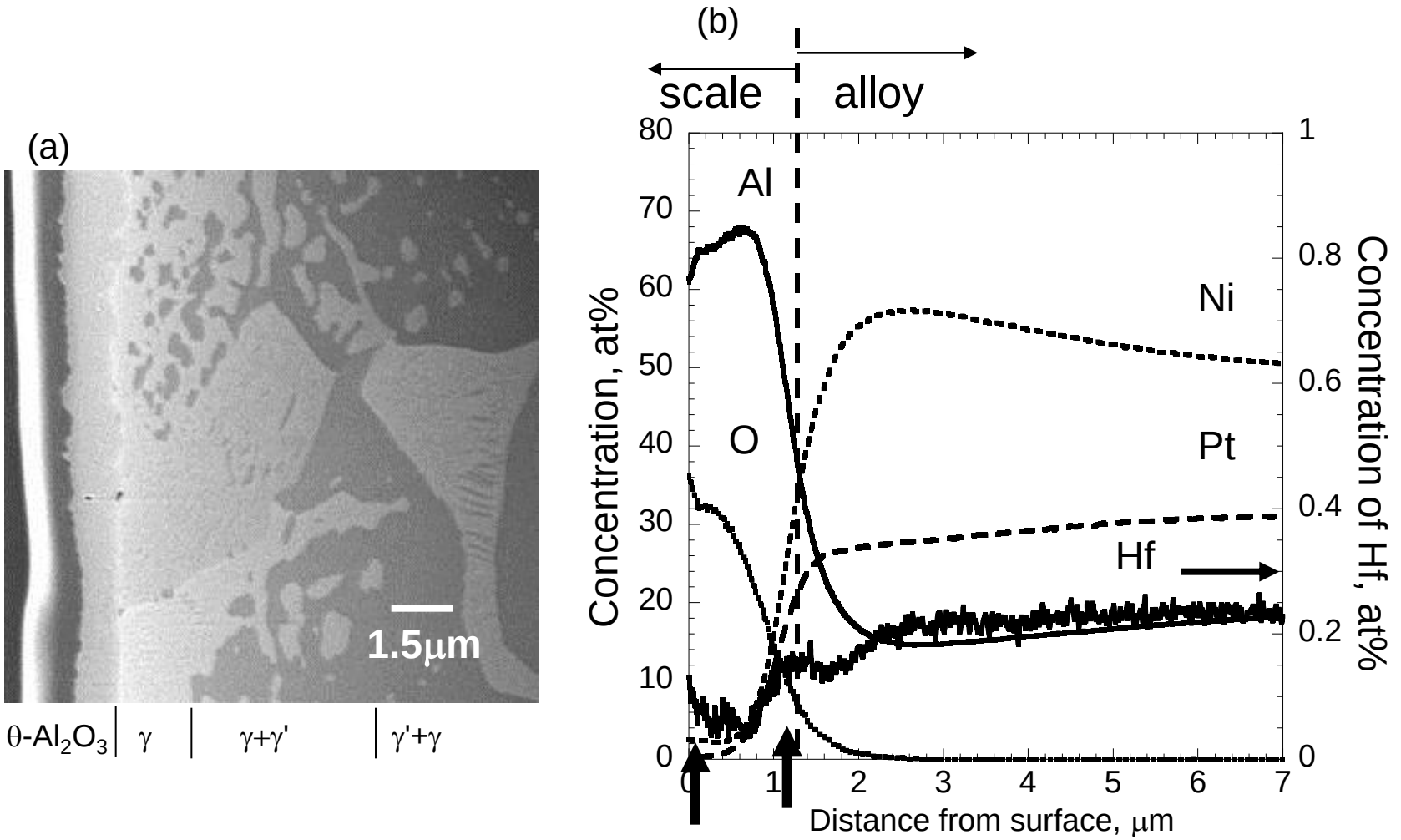

Fig. 10 Hf enrichment at the scale/alloy interface due to formation of Al-depleted γ at alloy subsurface region. (a) SIM image of Ni-22Al-30Pt-0.5Hf alloy after 30min of isothermal oxidation, (b) Depth profiles of each element by GD-OES analysis

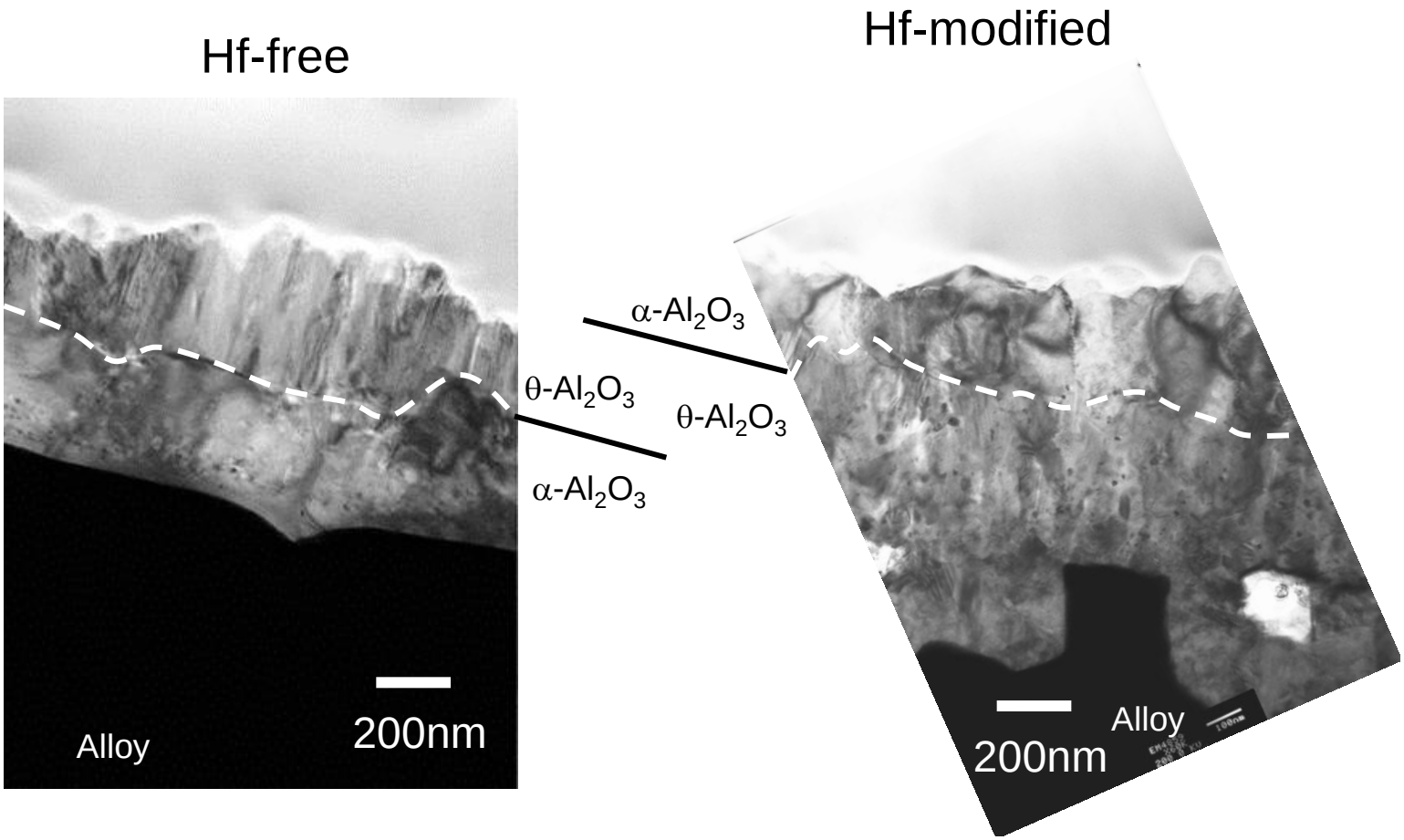

Fig. 11 Different order of duplex Al_2O_3 layers developed on the alloys with and without Hf after 39 oxidation cycles (115min total). Images are re-arranged from Fig. 7b and Fig. 9b for Hf-free and Hf-modified alloys, respectively.